ARMY RESEARCH LABORATORY

Navier-Stokes Predictions of Pitch-Damping for a Family of Flared Projectiles

Paul Weinacht

ARL-TR-591 October 1994

NOTICES

Destroy this report when it is no longer needed. DO NOT return it to the originator.

Additional copies of this report may be obtained from the National Technical Information Service, U.S. Department of Commerce, 5285 Port Royal Road, Springfield, VA 22161.

The findings of this report are not to be construed as an official Department of the Army position, unless so designated by other authorized documents.

The use of trade names or manufacturers' names in this report does not constitute indorsement of any commercial product.

REPORT DOCUMENTATION PAGE

Form Approved
OMB No. 0704-0188

1. AGENCY USE ONLY *(Leave blank)*	2. REPORT DATE	3. REPORT TYPE AND DATES COVERED
	October 1994	Final, January 1989 - June 1993

4. TITLE AND SUBTITLE
Navier-Stokes Predictions of Pitch-Damping for a Family of Flared Projectiles

5. FUNDING NUMBERS
PR: 1L161102AH43

6. AUTHOR(S)
Paul Weinacht

7. PERFORMING ORGANIZATION NAME(S) AND ADDRESS(ES)
U.S. Army Research Laboratory
ATTN: AMSRL-WT-PB
Aberdeen Proving Ground, MD 21005-5066

8. PERFORMING ORGANIZATION REPORT NUMBER

9. SPONSORING/MONITORING AGENCY NAMES(S) AND ADDRESS(ES)
US Army Research Laboratory
ATTN: AMSRL-OP-AP-L
Aberdeen Proving Ground, MD 21005-5066

10.SPONSORING/MONITORING AGENCY REPORT NUMBER
ARL-TR-591

11. SUPPLEMENTARY NOTES

12a. DISTRIBUTION/AVAILABILITY STATEMENT
Approved for public release; distribution is unlimited.

12b. DISTRIBUTION CODE

13. ABSTRACT *(Maximum 200 words)*

A parabolized Navier-Stokes approach has been applied to predict the pitch-damping force and moment coefficients for a family of flared projectiles. This family of flared projectiles, which has been tested in the Army Research Laboratory's (ARL) Aerodynamics Range, consists of a common forebody with various flared afterbodies including straight flares, biconic flares, straked flares, and flares with finlets. The predicted pitch-damping force and moment coefficients are determined from the aerodynamic side force and moment acting on the projectiles due to steady coning motion. The predictions of the flow field about the projectiles undergoing steady coning motion are accomplished using a rotating coordinate frame which rotates at the coning rate of the projectile. The governing equations have been modified to include the centrifugal and Coriolis force terms due to the rotating coordinate frame. The predictions of the pitch-damping moment coefficient are compared with pitch-damping coefficients determined from the inflight motion of the projectile. The predictions of the pitch-damping moment coefficients are in good agreement with the range data.

14. SUBJECT TERMS	15. NUMBER OF PAGES
Projectiles, Aerodynamic Characteristics, Computational Fluid Dynamics, Pitch-Damping	29
	16. PRICE CODE

17. SECURITY CLASSIFICATION OF REPORT	18. SECURITY CLASSIFICATION OF THIS PAGE	19. SECURITY CLASSIFICATION OF ABSTRACT	20. LIMITATION OF ABSTRACT
UNCLASSIFIED	UNCLASSIFIED	UNCLASSIFIED	SAR

INTENTIONALLY LEFT BLANK.

Table of Contents

INTENTIONALLY LEFT BLANK.

List of Figures

INTENTIONALLY LEFT BLANK.

I. INTRODUCTION

The aerodynamics of a family of flared projectiles has been investigated experimentally[1, 2] in the Ballistic Research Laboratory[1] Aerodynamics Range. These projectiles are possible concepts for a 25mm training round. Predictive techniques have also been applied to examine the drag and static pitch-plane aerodynamics of these rounds.[2] In this report, an approach for predicting the pitch-damping aerodynamics coefficients has been applied to this family of projectiles. This approach has been previously applied to predict the pitch-damping of both finned projectiles[3] and axisymmetric shell.[4]

A schematic of the baseline cone-cylinder-flare projectile configuration is shown in Figure 1. Each of the projectiles examined here has the same cone-cylinder forebody. The forebody has a slightly truncated conical nose. In the computations, the nose is modeled as a sharp tipped cone. The cylindrical portion of the body also has a number of subcaliber grooves which permit the launch loads to be transferred from the sabot to the projectile during launch. These grooves are not modeled in the computations presented here.

Various afterbodies have been analyzed both experimentally and computationally. Schematics of the afterbodies are shown in Figure 2. Additional dimensions are listed in Table 1. The configurations CS-V4-2 through CS-V4-5 have a 1-caliber afterbody extention added to the baseline configuration, CS-V4-1. The angle of inclination of the conical extentions for configurations CS-V4-2 through CS-V4-5 are, respectively, 6° (simple extention of original flare), 0° (cylindrical skirt), 12° (steeper flare), and −6° (boattail). Configuration CS-V4-6 consists of 9.37° flare which has been machined to produce a square cross section over the last caliber of the body. Configuration CS-V4-7 is identical to the boattailed configuration CS-V4-5, except that four 12° fins have been added to the boattailed portion of the body. The fins are 0.153 calibers thick. The final configuration, CS-V4-8, is identical to the baseline configuration, except that four boundary layer strakes have been added to the flared portion of the body. The strakes are 0.153 calibers in height and width.

The flared portion of the bodies have been hollowed to shift the center of gravity forward to produce statically stable configurations. There is some evidence that the hollow base may have some effect on the aerodynamics. In this investigation, the flow field in the base region has not been computed, hence, the effect of the hollow base on the aerodynamics cannot be assessed.

II. THEORETICAL BACKGROUND

By applying linear flight mechanics theory such as that developed by Murphy,[5] it can be shown that aerodynamic side force and moment coefficients acting on a projectile in steady coning motion can be related to the pitch-damping force and moment coefficients. Steady coning motion is defined as the motion performed by a missile flying at a constant angle with respect to the free-stream velocity vector and undergoing a rotation at a constant

[1]The U.S. Army Ballistic Research Laboratory was deactivated on 30 September 1992 and subsequently became a part of the U.S. Army Research Laboratory (ARL) on 1 October 1992.

angular velocity about a line parallel to the free-stream velocity vector and coincident with the projectile center of gravity (Figure 3). Coning motion is, in fact, a specific combination of two orthogonal planar pitching motions. The use of steady coning motion to determine the pitch-damping aerodynamic coefficients provides an interesting and cost-effective approach for determining the aerodynamics which are normally associated with unsteady or time-dependent motions.

Previously, Tobak, Schiff, and Peterson[6] examined the aerodynamics of bodies of revolution in coning motion and proposed that the nonlinear aerodynamic forces and moments acting on a body performing large amplitude nonplanar motions could be composed of four characteristic motions: (1) steady angle of attack, (2) pitching motion, (3) rolling motion, and (4) coning motion. Typically, the linear aerodynamic force and moment formulation considers only forces and moments due to the first three motions, and assumes that a nonplanar motion can be described by the vector sum of two independent planar motions. The addition of coning motion allows for coupling between planar motions in the nonlinear formulation. Their nonlinear theory also confirms the linear theory result that the side force and moment due to coning motion is related to the linear pitch-damping coefficients. Schiff and Tobak[7] performed wind tunnel experiments on a conical body undergoing separate or combined spinning and coning motions to provide additional validation for the theory.

As part of the development, Schiff[8] computed the supersonic inviscid flow about a conical body undergoing coning motion. To compute the flow around the body in coning motion, Schiff made use of a rotating coordinate frame. Within the rotating coordinate frame the flow was steady, thus the steady Euler equations could be solved. The governing equations were modified to include the centrifugal and Coriolis force terms. His computed results compared well with experimental results and with estimates of pitch-damping coefficients using a linear theory. Later studies by Agarwal and Rakich[9] and Lin[10] also employed rotating coordinate frames to compute the supersonic viscous flow about conical bodies in coning motion. More recently, Weinacht and Sturek[3] performed computations for finned projectiles in coning motion to determine the pitch-damping coefficients.

In each of these efforts, the pitch-damping coefficients were determined from the side moment due to lunar coning motion. Lunar coning motion is a specific form of coning motion in which the body does not rotate with respect to the pitch plane. The relation between the side moment due to lunar coning motion and the pitch-damping moment is shown in equation 1 without derivation. This expression was obtained using linear flight mechanics theory (details can be found in reference [4]) and is essentially the same as that obtained earlier by Schiff and Tobak[7] by applying their nonlinear theory to bodies of revolution.

$$C_n = \delta(\frac{\dot{\phi}l}{V})(\gamma C_{n_{p\alpha}} + [C_{m_q} + \gamma C_{m_{\dot{\alpha}}}]) \tag{1}$$

The side moment in the coning frame of reference, C_n, varies linearly with the coning rate, $\dot{\phi}$, and the sine of the angle of attack, δ, and is a function of the pitch-damping moment coefficient, $C_{m_q} + \gamma C_{m_{\dot{\alpha}}}$, and the Magnus moment coefficient, $C_{n_{p\alpha}}$. The cosine of the angle of attack, γ, is often dropped because it is close to one in the region where linear theory is valid. In many cases, the Magnus moment coefficient is much smaller than the pitch-damping coefficient, and the Magnus moment can be dropped allowing the side moment due to lunar coning to be directly related to the pitch-damping moment coefficient.

Recently, Weir.cht, Sturek, and Schiff[4] computed the pitch-damping for axisymmetric shell using a specific combination of spinning and coning motion which allows the pitch-damping force and moment coefficients to be directly related to the side force and moment due to this motion, as shown in equation 2.

$$C_n = \delta(\frac{\dot{\phi}l}{V})[C_{m_q} + \gamma C_{m_\alpha}] \tag{2}$$

In the coning coordinate frame, the body will spin in the opposite direction of the coning motion, where the spin rate in the coning frame, p_{cf} is related to the coning rate in the following manner; $p_{cf} = -\gamma\dot{\phi}$. Despite the simplicity of this expression, the Magnus problem has not been entirely removed from the problem, however. This is because the motion in the coning coordinate frame involves coning and spinning motions. Thus, any approach, whether it be computational or experimental, which uses this motion must be capable of modeling both of these effects.

Similar expressions which relate the side force due to coning to the pitch-damping force and Magnus force can be derived for the cases of lunar coning and combined spinning and coning motion.

III. COMPUTATIONAL APPROACH

Computation of the viscous flow field about the flared projectile configurations was accomplished by solving the thin-layer Navier-Stokes equations using the parabolized Navier-Stokes technique of Schiff and Steger.[11] Using the parabolized Navier-Stokes technique, computational results are obtained by marching through the grid from the projectile nose to the base. This technique is applicable in the supersonic flow regime and requires that the flow field contain no regions of flow separation in the axial direction. Because the computational approach requires only a single sweep through the computational grid, it is very efficient compared with time-marching approaches which require many sweeps through the grid.

The flow field predictions of the projectile in steady coning motion have been performed using a rotating coordinate frame which rotates at the coning rate of the projectile. The fluid flow relative to the rotating coordinate frame does not vary with time, allowing the steady (non-time varying) Navier-Stokes equations to be applied. To implement the rotating coordinate frame, the governing equations have been modified to include the effect of centrifugal and Coriolis forces. The steady thin-layer Navier-Stokes equations are shown in equation 3.

$$\frac{\partial \hat{E}}{\partial \xi} + \frac{\partial \hat{F}}{\partial \eta} + \frac{\partial \hat{G}}{\partial \zeta} + \hat{H} = \frac{1}{Re}\frac{\partial \hat{S}}{\partial \zeta} \tag{3}$$

Here, $\hat{E}$, $\hat{F}$, and $\hat{G}$ are the inviscid flux vectors, $\hat{S}$ is the viscous flux vector, and $\hat{H}$ is the source term containing the Coriolis and centrifugal force terms which result from the rotating coordinate frame. Each of these matrices are functions of the dependent variables represented by the vector $q(\rho, \rho u, \rho v, \rho w, e)^T$, where ρ and e are the density and the total energy per unit volume, and u, v, and w, are the velocity components in x, y, and z directions. The pitch

plane is oriented in the $x-z$ plane. The flux terms are shown in equation 4.

$$\hat{E} = \frac{1}{J}\begin{bmatrix} \rho U \\ \rho u U + \xi_x p \\ \rho v U \\ \rho w U \\ (e+p)U \end{bmatrix} \quad \hat{F} = \frac{1}{J}\begin{bmatrix} \rho V \\ \rho u V + \eta_x p \\ \rho v V + \eta_y p \\ \rho w V + \eta_z p \\ (e+p)V \end{bmatrix} \quad \hat{G} = \frac{1}{J}\begin{bmatrix} \rho W \\ \rho u W + \zeta_x p \\ \rho v W + \zeta_y p \\ \rho w W + \zeta_z p \\ (e+p)W \end{bmatrix}$$

$$\hat{H} = \frac{1}{J}\begin{bmatrix} 0 \\ H_2 \\ H_3 \\ H_4 \\ H_5 \end{bmatrix} \quad \hat{S} = \frac{1}{J}\begin{bmatrix} 0 \\ m_1 \frac{\partial u}{\partial \zeta} + m_2 \zeta_x \\ m_1 \frac{\partial v}{\partial \zeta} + m_2 \zeta_y \\ m_1 \frac{\partial w}{\partial \zeta} + m_2 \zeta_z \\ m_3 \end{bmatrix} \tag{4}$$

where

$$\begin{aligned} H_2 &= -2\Omega_c \rho v \sin\alpha - \rho\Omega_c^2 (x - x_{cg}) \sin^2\alpha + \rho\Omega_c^2 z \sin\alpha\cos\alpha \\ H_3 &= 2\Omega_c \rho u \sin\alpha - 2\Omega_c \rho w \cos\alpha - \rho\Omega_c^2 y \sin^2\alpha - \rho\Omega_c^2 y \cos^2\alpha \\ H_4 &= 2\Omega_c \rho v \cos\alpha + \rho\Omega_c^2 (x - x_{cg}) \sin\alpha\cos\alpha - \rho\Omega_c^2 z \cos^2\alpha \\ H_5 &= (-\Omega_c^2 (x - x_{cg}) \sin^2\alpha + \Omega_c^2 z \sin\alpha\cos\alpha)\rho u - (\Omega_c^2 y \sin^2\alpha + \Omega_c^2 y \cos^2\alpha)\rho v \\ &\quad + (\Omega_c^2 (x - x_{cg}) \sin\alpha\cos\alpha - \Omega_c^2 z \cos^2\alpha)\rho w \end{aligned} \tag{5}$$

$$\begin{aligned} U &= u\xi_x \\ V &= u\eta_x + v\eta_y + w\eta_z \\ W &= u\zeta_x + v\zeta_y + w\zeta_z \end{aligned} \tag{6}$$

$$\begin{aligned} m_1 &= (\mu + \mu_t)(\zeta_x^2 + \zeta_y^2 + \zeta_z^2) \\ m_2 &= \frac{1}{3}(\mu + \mu_t)(\zeta_x \frac{\partial u}{\partial \zeta} + \zeta_y \frac{\partial v}{\partial \zeta} + \zeta_z \frac{\partial w}{\partial \zeta}) \\ m_3 &= \frac{1}{(\gamma - 1)}(\frac{\mu}{Pr} + \frac{\mu_t}{Pr_t})(\zeta_x^2 + \zeta_y^2 + \zeta_z^2)\frac{\partial a^2}{\partial \zeta} + \frac{1}{2} m_1 \frac{\partial q^2}{\partial \zeta} \\ &\quad + m_2(u\zeta_x + v\zeta_y + w\zeta_z) \end{aligned} \tag{7}$$

$$a^2 = \frac{\gamma p}{\rho} \tag{8}$$

$$q^2 = u^2 + v^2 + w^2 \tag{9}$$

$$\begin{aligned} &\xi_x = \tfrac{1}{x_\xi} \\ &\eta_x = J(z_\xi y_\zeta - y_\xi z_\zeta) \qquad \eta_y = J(x_\xi z_\zeta) \quad \eta_z = J(-x_\xi y_\zeta) \\ &\zeta_x = J(y_\xi z_\eta - z_\xi y_\eta) \qquad \zeta_y = J(-x_\xi z_\eta) \quad \zeta_z = J(x_\zeta y_\eta) \\ &J = 1/\left(x_\xi (y_\eta z_\zeta - y_\zeta z_\eta)\right) \end{aligned} \tag{10}$$

The pressure, p, can be related to the dependent variables by applying the ideal gas law.

$$p = (\gamma - 1)\left[e - \frac{\rho}{2} q^2\right] \tag{11}$$

The turbulent viscosity, μ_t, which appears in the viscous matrices, was computed using the Baldwin-Lomax turbulence model.[12]

The thin-layer equations are solved using the parabolized Navier-Stokes technique of Schiff and Steger.[11] Following the approach of Schiff and Steger, the governing equations, which have been modified here to include the Coriolis and centrifugal force terms, are solved using a conservative, approximately factored, implicit finite-difference numerical algorithm as formulated by Beam and Warming.[13] Further details on the implementation of the source terms due to rotating coordinate frame can be found in references [3] and [4].

The computations presented here were performed using a shock-fitting procedure reported by Rai and Chaussee.[14] This procedure solves the five Rankine-Hugoniot jump conditions, two geometric shock-propagation conditions, and one compatibility equation to determine the values of the five dependent variables immediately behind the shock, as well as the position of the shock. By including the implicit part of the source term due to the rotating coordinate frame in the circumferential inversion, the shock-fitting procedure of Rai and Chaussee can be used without modification, as long as the correct free-stream conditions are specified as shown in equation 12 in nondimensional form.

$$\begin{aligned}
\rho &= 1 \\
\rho u &= M_\infty cos\alpha + y\Omega_c \sin\alpha \\
\rho v &= \Omega_c(z\cos\alpha - (x - x_{cg})\sin\alpha) \\
\rho w &= M_\infty sin\alpha - y\Omega_c \cos\alpha \\
e &= p_\infty/(\gamma - 1) + \frac{1}{2}\{(M_\infty cos\alpha + y\Omega_c \sin\alpha)^2 \\
&\quad +(\Omega_c(z\cos\alpha - (x - x_{cg})\sin\alpha))^2 + (M_\infty sin\alpha - y\Omega_c \cos\alpha)^2\}
\end{aligned} \tag{12}$$

On the body surface, constant (ambient) wall temperature, no-slip boundary conditions were applied. For the cases involving spin, the horizontal and vertical velocities at the projectile surface were appropriately modified to account for the tangential velocity due to solid body rotation.

IV. RESULTS

Using side force and moment due to steady lunar coning motion, predictions of the pitch-damping force and moment coefficients have been made for the family of flare projectiles. The computations were performed over a range of Mach numbers (M_∞ = 3.0 to 4.5) for free-flight (sea-level) atmospheric conditions.

The computed variation of the side moment coefficient with coning rate for configuration CS-V4-1 at Mach 4 and 2° angle of attack is shown in Figure 4. The variation is linear over the range of coning rates examined here, and the slope, $C_{n_{\dot{\phi}}}$, can be determined without any ambiguity. The range of coning rates considered here encompasses the pitching frequency of the projectile.

Figure 5 shows the variation of the side moment slope, $C_{n_{\dot{\phi}}}$, with angle of attack for configuration CS-V4-1. The angle of attack variation is seen to be linear up to about 5° angle

of attack. At angles of attack less than 5°, the normalized side moment slope, C_{n_ϕ}/δ, varies by only a few percent as the angle of attack changes. Beyond 5° angle of attack, the side moment shows a strong nonlinear behavior with angle of attack. In the development of the relation between the side moment due to coning and the pitch-damping moment, the aerodynamic coefficients were assumed to vary linearly with angle of attack. At angles of attack greater than 5°, the previously presented relation between the pitch-damping coefficients and the side force and moment due to coning motion may no longer be valid.

From the side moment slope normalized by the sine of the angle of attack, the pitch-damping coefficients as a function of Mach number were determined for each of the eight flared configurations. The predictions were obtained at 5° angle of attack. Figures 6-13 display the predictions of the pitch-damping moment coefficients, as well as the pitch-damping moment coefficients determined from the free flight range tests. The predictions of the pitch-damping moment are within the accuracy of the range measurements. The predicted pitch-damping moment coefficients for each of the configurations show a weak dependence on Mach number over the range of Mach numbers considered here.

Figure 14 shows a comparison of the pitch-damping moment coefficients for each of the eight configurations at Mach 4. Both the PNS predictions and the range data are shown. Each of the bodies with the conical extentions, configurations CS-V4-2 through CS-V4-5, have larger pitch-damping coefficients compared with the baseline configuration CS-V4-1. Computational predictions show a consistent increase in the pitch-damping for the bodies with the conical extentions with the boattailed configuration having lowest pitch-damping coefficient and the steepest flare having the highest pitch-damping coefficient. These trends are, for the most part, reflected by the range data.

The finned configuration, which is identical to the boattailed configuration except that four 12° swept fins have been added to the boattailed portion of the body, shows a modest increase in the damping over the boattailed configuration. The finned configuration, however, produces significantly less pitch-damping than the configuration with the 12° flare extention. Again, these trends are reflected by the range data. The configuration with the boundary layer strakes also produces a modest increase in the damping compared with the baseline configuration which has no strakes. The square base configuration (CS-V4-6), which has the same base area as the baseline configuration (CS-V4-1) and the configuration with the cylindrical skirt (CS-V4-3), produces more damping than the baseline configuration and slightly more damping than the cylindrical skirt.

In addition to pitch-damping moment coefficient, predictions of the the pitch-damping force coefficient have been made. The pitch-damping force coefficient can be determined from the side force variation with coning rate normalized by the sine of the angle of attack. The predicted variation of the pitch-damping force coefficient with Mach number for configuration CS-V4-1 is shown in Figure 15. This coefficient is seen to decrease with increasing Mach number for the range of Mach numbers considered here. The Mach number variation was typical of that observed for each of the eight configurations. The pitch-damping force coefficient produces little effect on the motion of the projectile and is very difficult to determine from the in-flight projectile motion. For this reason no range data are shown. Although the pitch-damping force coefficient is not required to determine the in-flight motion, this coefficient can be useful in determining the variation of the pitch-damping moment coefficient

with change in center of gravity. For this reason, a predictive approach for determining this coefficient is of interest.

Determining the pitch-damping coefficients from the side force and moment due to lunar coning motion requires that the Magnus force and moment be determined from another source or neglected. For the axisymmetric configurations (CS-V4-1 to CS-V4-5), the Magnus force and moment have been predicted using the PNS approach. These calculations were performed with the body spinning at angle of attack and in the absence of coning motion. Magnus predictions for the non-axisymmetric geometries could not be made because the combination of spin and angle of attack for these bodies produces a time-dependent flow field. Figures 16 and 17 shows the predicted Magnus force and moment as a function of Mach number for each of the axisymmetric configurations. The configuration with the boattailed afterbody shows the largest positive Magnus moment, while the 12° flared afterbody shows the largest negative Magnus moment. These two configurations also produce the smallest and largest Magnus force coefficients. Figure 18 shows a comparison of the Magnus moment coefficients by configuration at Mach 4. Range results are shown for each of the eight configurations, while computational results are shown for the axisymmetric configurations. The computational data are bracketed by the range data for each of the axisymmetric configurations, and similar trends are shown by the computational and experimental results. Both the computational and experimental results reveal that the Magnus moment is small in comparison to the pitch-damping moment coefficient for the configurations examined here. The computational predictions also confirm that the Magnus force is small in relation to the pitch-damping force coefficient. This result demonstrates that, by ignoring the contribution from the Magnus coefficients, the pitch-damping coefficients can be determined directly from the side force and moment due to lunar coning motion with little effect on the accuracy of the prediction.

For the axisymmetric configurations, calculations were also performed using combined spinning and coning motion. The predicted pitch-damping coefficients, which are obtained directly from the normalized side force and moment (Equation 2), showed differences of less than 0.02 % with results obtained by subtracting the Magnus coefficients from the normalized side force and moment coefficients due to lunar coning motion (Equation 1). This result demonstrates the lack of coupling between coning motion and spin over the range of spin and coning rates considered here for small angles of attack.

The Magnus moment predictions shown here are interesting because the predictions show that the sign of the Magnus moment is dependent on the projectile geometry. The Magnus moment results from an interaction between spin and angle of attack which causes a three dimensional boundary layer displacement effect. The magnitude of the effect is greatest near the aft end of the body where the boundary layer is thickest. Using the ballistic force-moment sign conventions, the result for axisymmetric shell is typically a negative Magnus force and a positive Magnus moment for cylindrical afterbodies with or without a boattail in supersonic flow. For three of the flared afterbodies, a negative Magnus moment is predicted, with the reversal in Magnus moment occurring over the flared portion of the body. A possible explanation for this phenomenon is that the boundary layer asymmetry produced by angle of attack and spin causes less side force on the side of the flare where the boundary layer is thickest due to a blanketing effect. The result is a positive contribution to the Magnus force and because this occurs at the aft end of the body, a negative contribution to the Magnus

moment is produced. This explanation appears to be supported by calculations which show that for these flared bodies, lift and pitching moment increases as the Reynolds number decreases, presumably due to a reduction in pressure on the lee side of the body caused by the thicker boundary layer.

V. CONCLUSION

The pitch-damping coefficients for a family of flared projectiles have been successfully computed using a parabolized Navier-Stokes approach. The pitch-damping force and moment coefficients have been predicted from the side force and moment due to steady lunar coning motion. The side moment is seen to vary linearly with coning rate across the range of interest. The side moment also varies linearly with angle of attack up to about 5°. These predictions provide a constraint on the range of angles of attack where the pitch-damping coefficients can be determined from the side force and moment due to coning. The pitch-damping moment coefficient predictions for the family of flared projectiles has been compared with data obtained from free-flight aerodynamics range tests and the comparisons show good agreement. The predictions show that the pitch-damping moment coefficient for these flared projectiles is relatively insensitive to Mach number at the range of supersonic velocities examined here. Predictions of the pitch-damping force coefficient have also been made, but no comparisons with range data are shown due to the small effect of this coefficient on the inflight motion of the projectile. The Magnus coefficients determined from the predictive approach and from range tests is seen to be small in relation to the pitch-damping coefficients. By ignoring the Magnus coefficients, the pitch-damping coefficients can be determined from the side force and moment due to lunar coning motion with little effect on the accuracy of the prediction.

Table 1. Physical Dimensions of the Family of Flared Projectiles

Configuration	Flare Angle	Flare Fineness Ratio	Extention (1 Caliber)	CG Position (Calibers from Base)	Total L/D
CS-V4-1	6.00°	3.51	None	7.55	15.36
CS-V4-2	6.00°	4.49	None	8.24	16.34
CS-V4-3	6.00°	4.49	6.0° Flare	8.36	16.34
CS-V4-4	6.00°	4.49	Cylindrical Skirt	8.13	16.34
CS-V4-5	6.00°	4.49	12.0° Flare	8.35	16.34
CS-V4-6	9.53°	4.49	6.0° Boattail	8.05	16.34
CS-V4-7	6.00°	4.50	Boattail with Fins	8.36	16.35
CS-V4-8	6.00°	3.50	Strakes	7.52	15.35

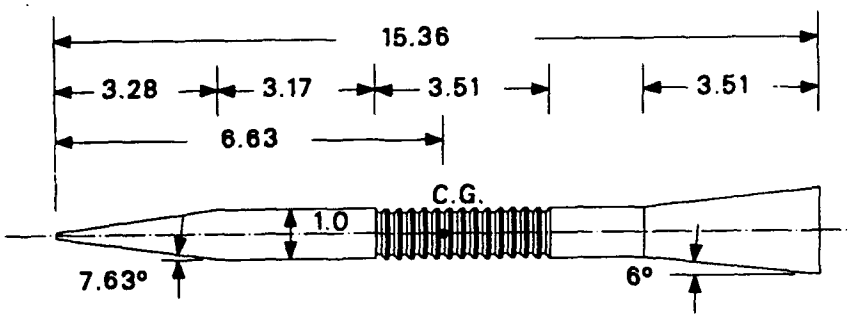

ALL DIMENSIONS IN CALIBERS (ONE CALIBER = 8.28 mm)

Figure 1. Schematic of baseline projectile configuration

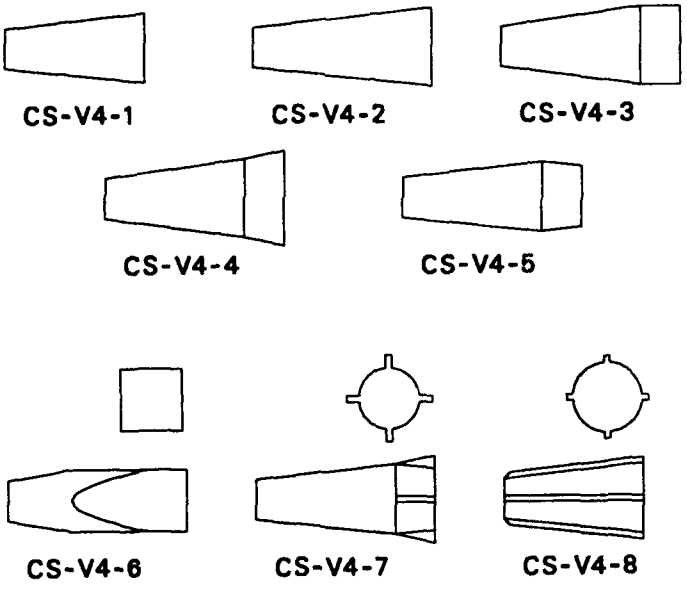

Figure 2. Schematic of projectile afterbodies

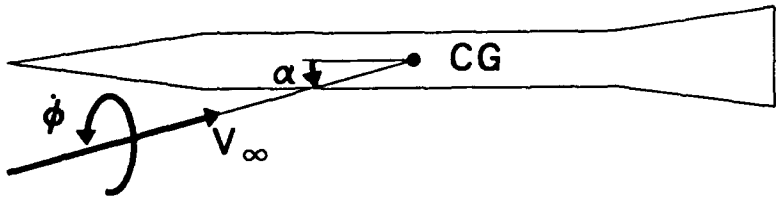

Figure 3. Schematic of coning motion

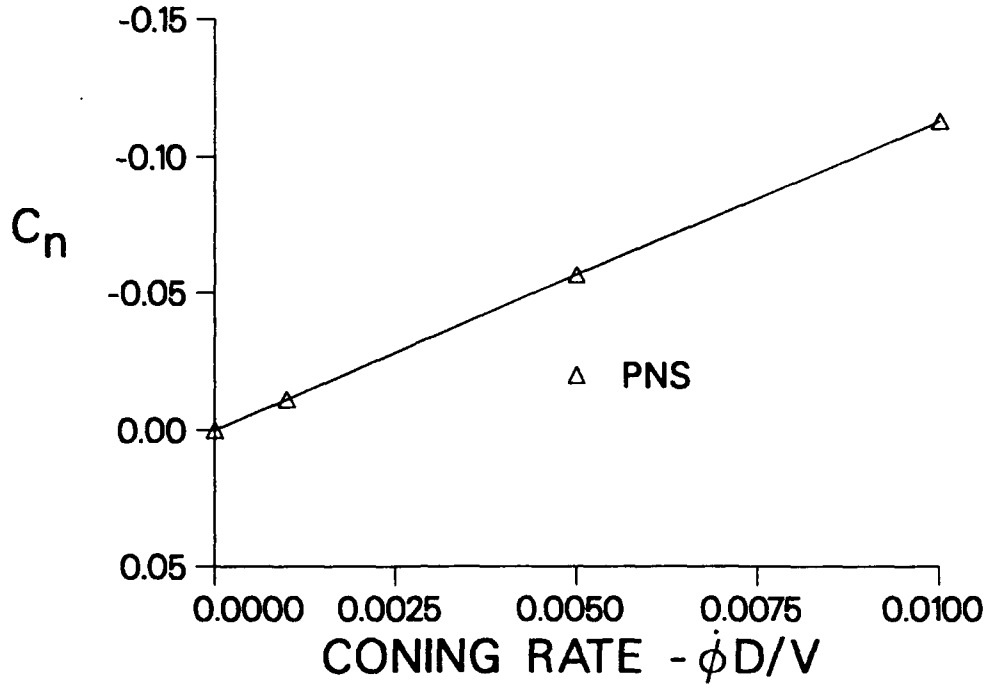

Figure 4. Variation of side moment coefficient with coning rate, CS-V4-1, Mach 4, $\alpha = 2.°$

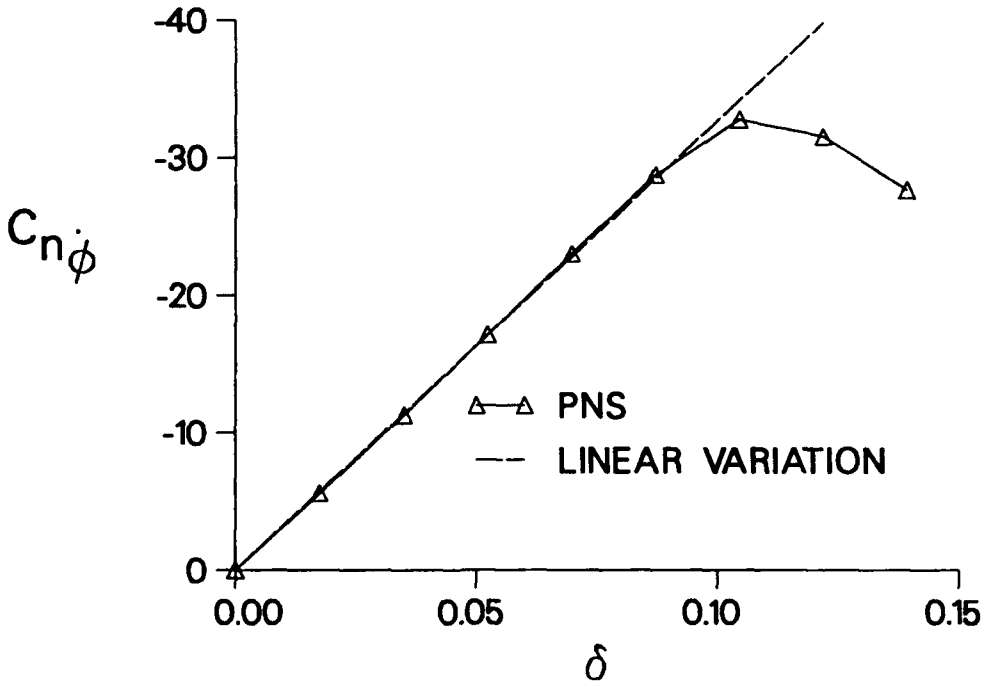

Figure 5. Variation of the side moment coefficient slope, $C_{n_{\dot{\phi}}}$, with the sine of the angle of attack, CS-V4-1, Mach 4

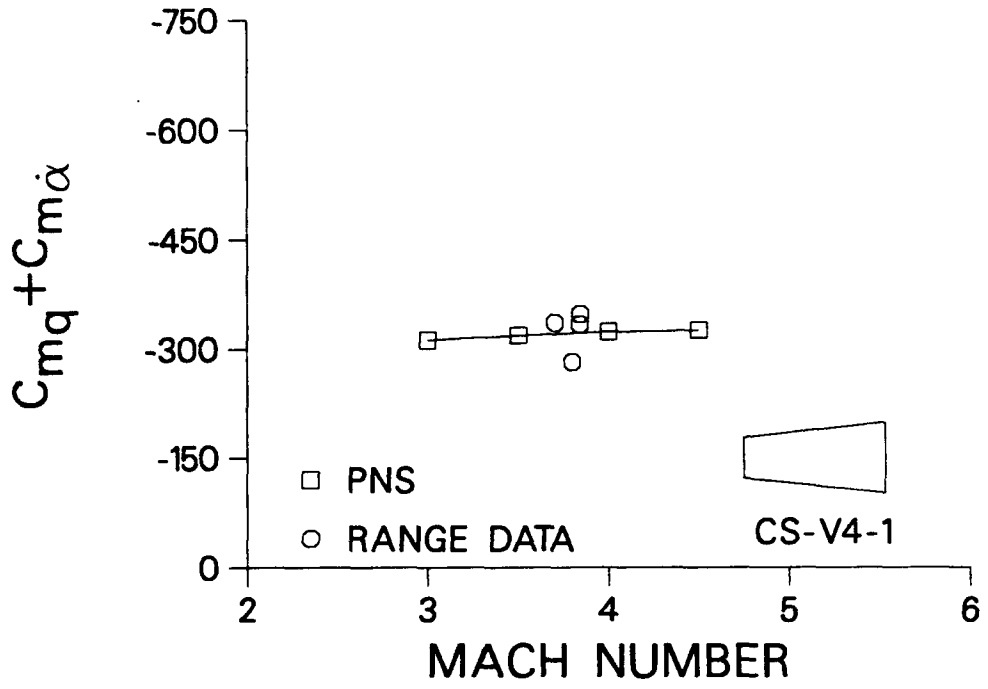

Figure 6. Variation of the pitch-damping moment coefficient with Mach number, CS-V4-1

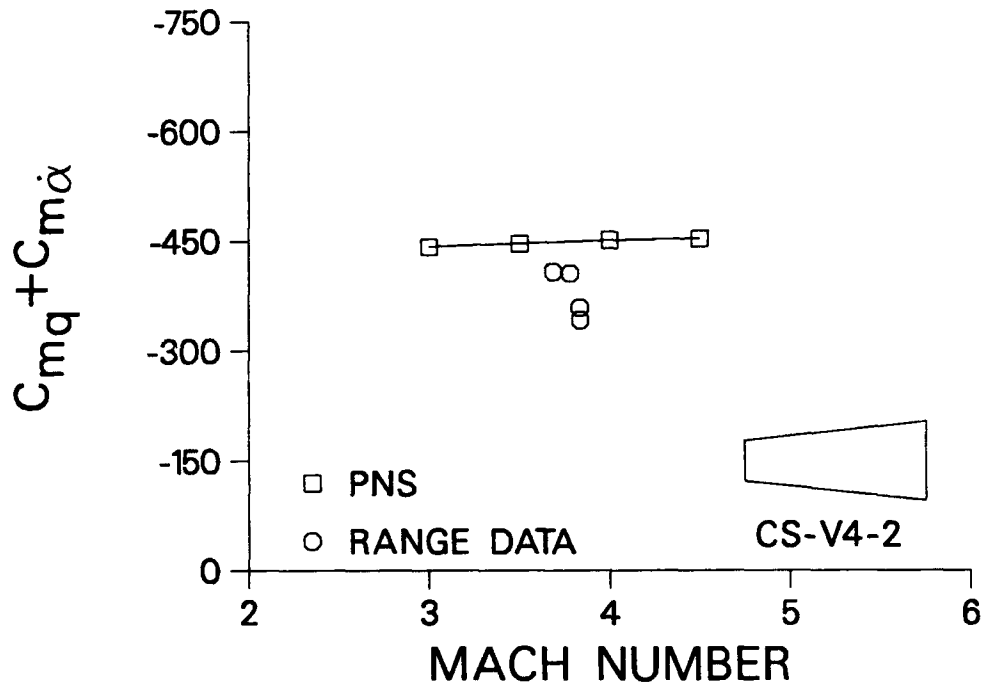

Figure 7. Variation of the pitch-damping moment coefficient with Mach number, CS-V4-2

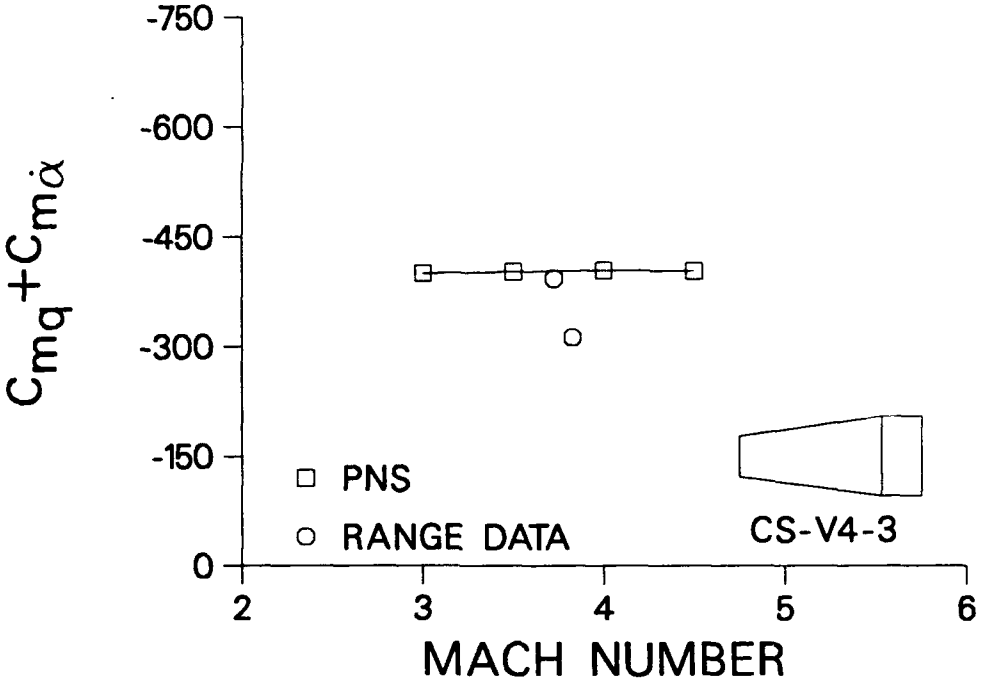

Figure 8. Variation of the pitch-damping moment coefficient with Mach number, CS-V4-3

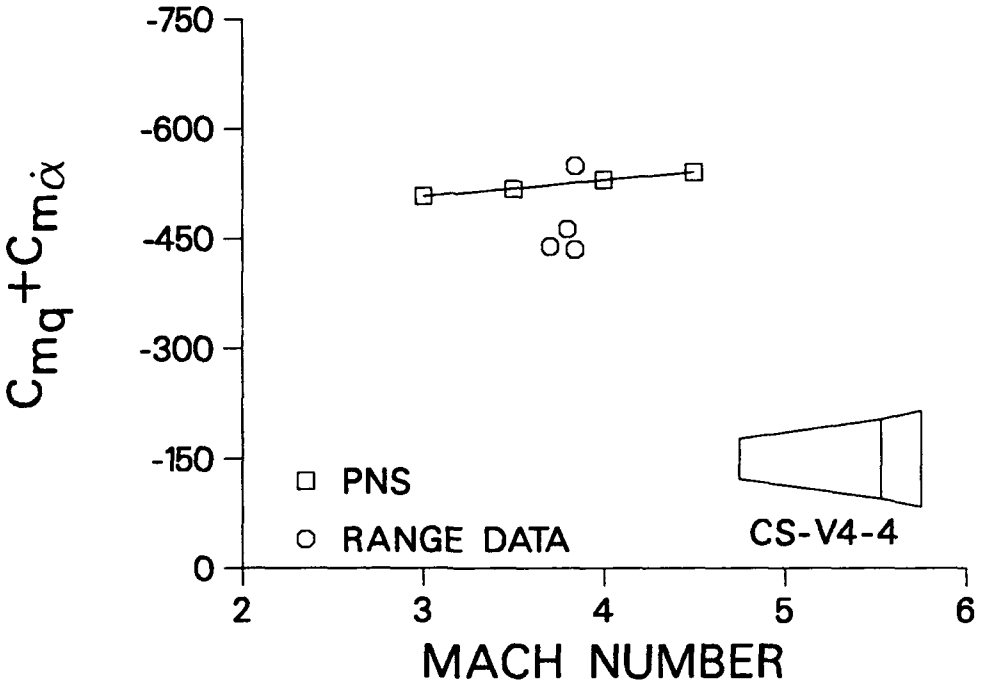

Figure 9. Variation of the pitch-damping moment coefficient with Mach number, CS-V4-4

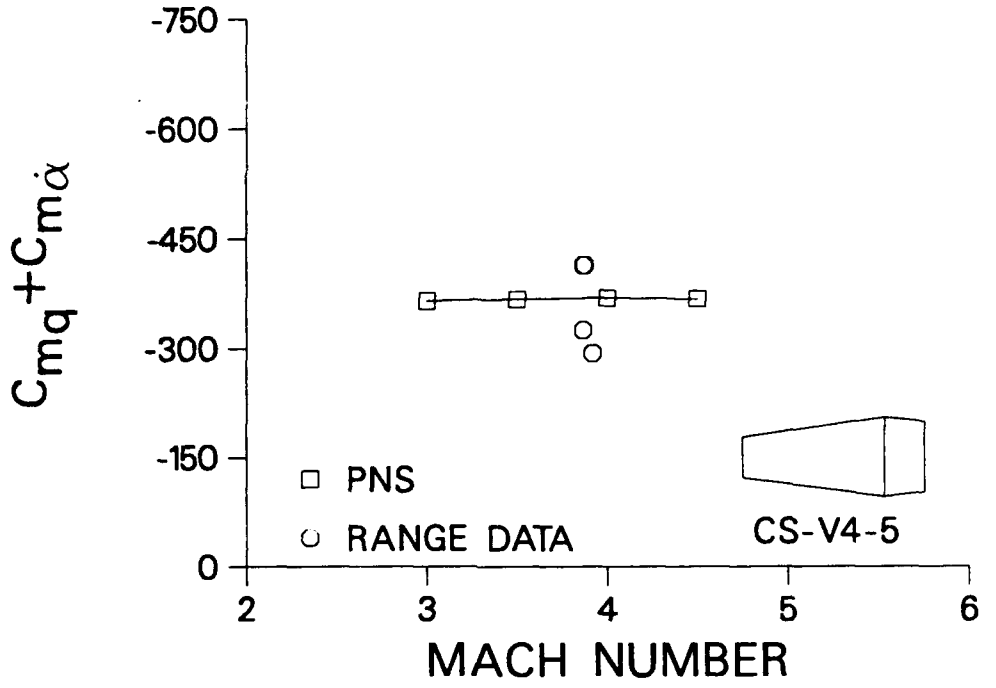

Figure 10. Variation of the pitch-damping moment coefficient with Mach number, CS-V4-5

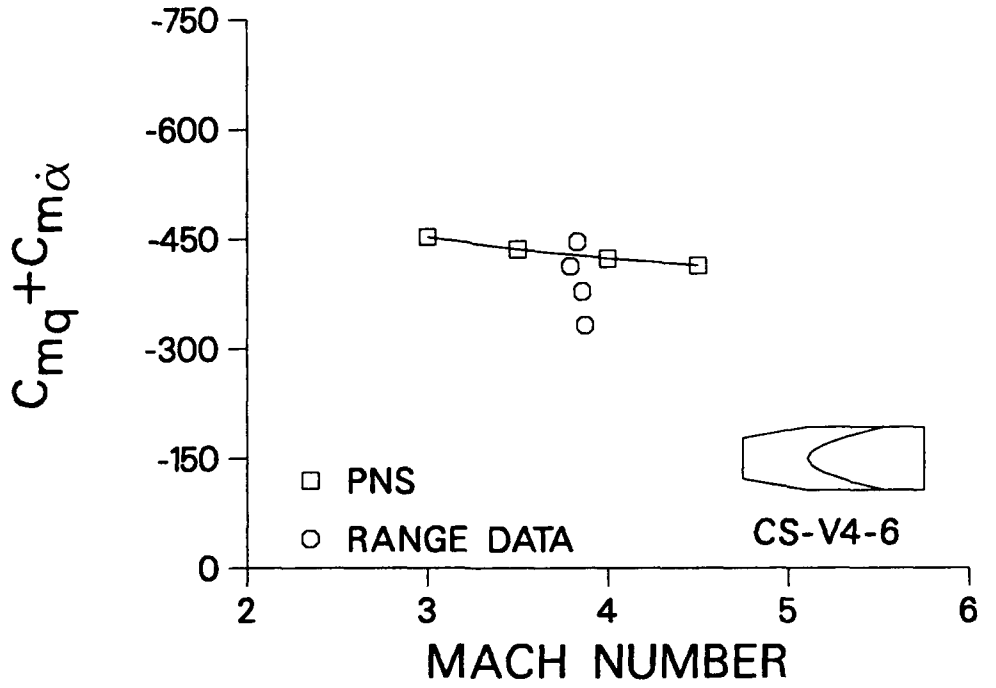

Figure 11. Variation of the pitch-damping moment coefficient with Mach number, CS-V4-6

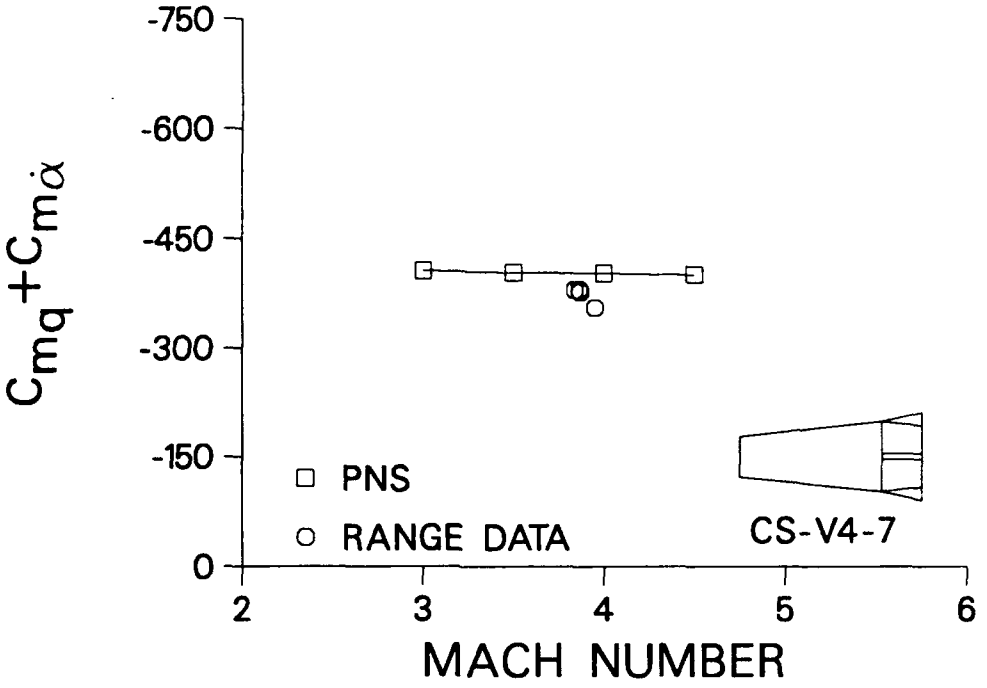

Figure 12. Variation of the pitch-damping moment coefficient with Mach number, CS-V4-7

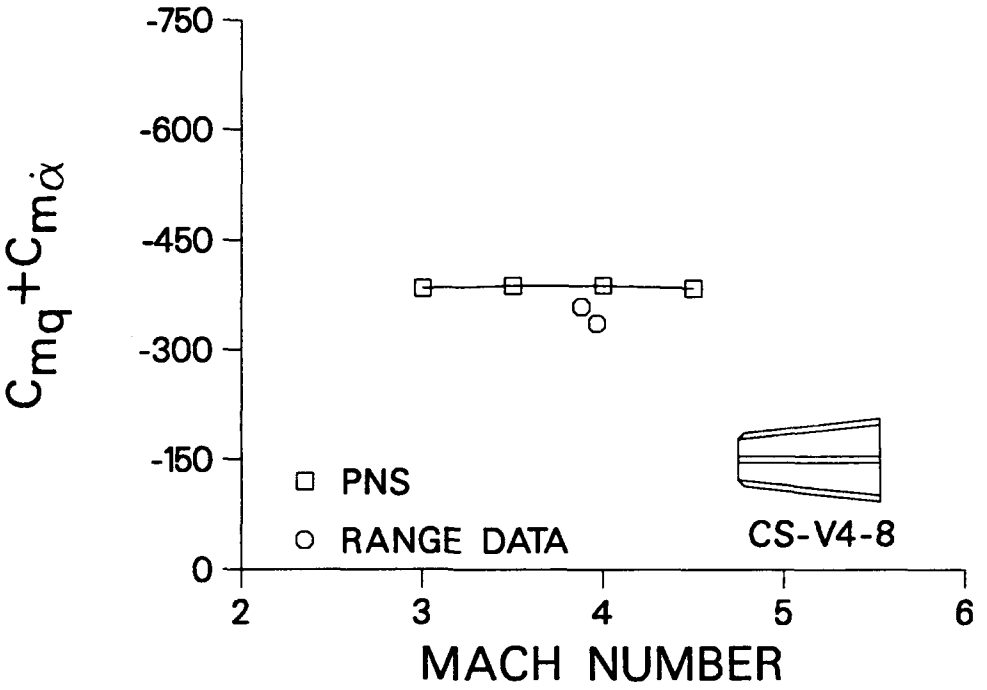

Figure 13. Variation of the pitch-damping moment coefficient with Mach number, CS-V4-8

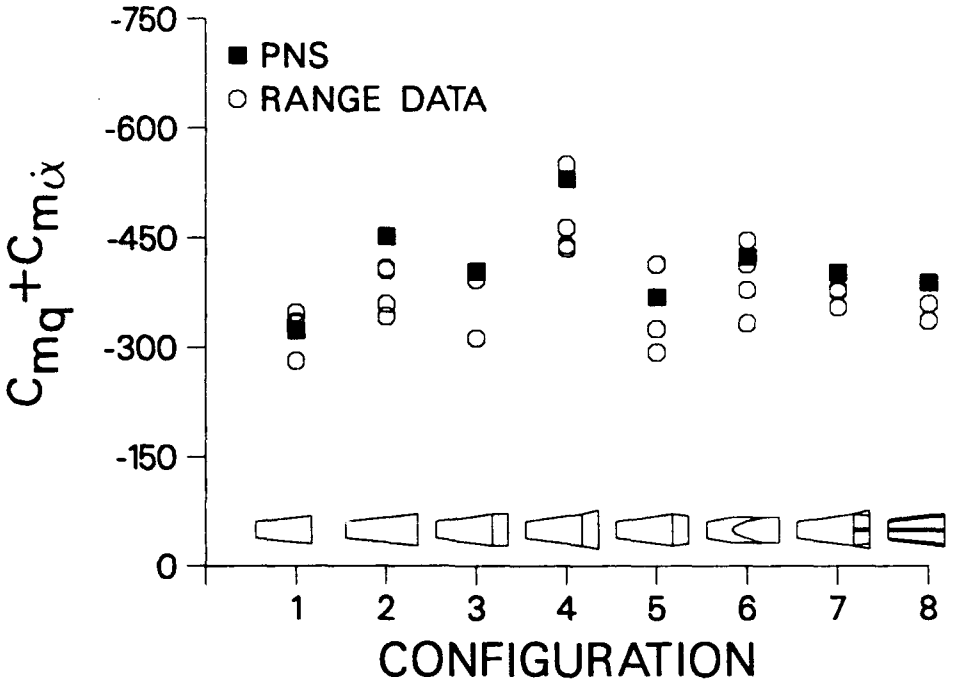

Figure 14. Pitch-damping moment coefficient versus configuration, Mach 4

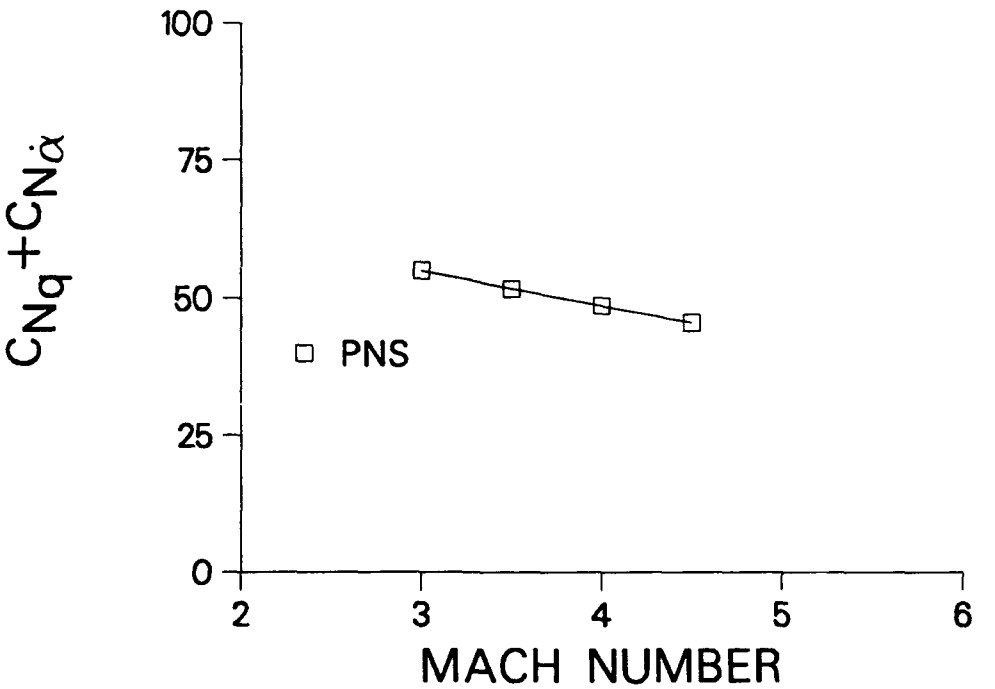

Figure 15. Variation of the pitch-damping force coefficient with Mach number, CS-V4-1

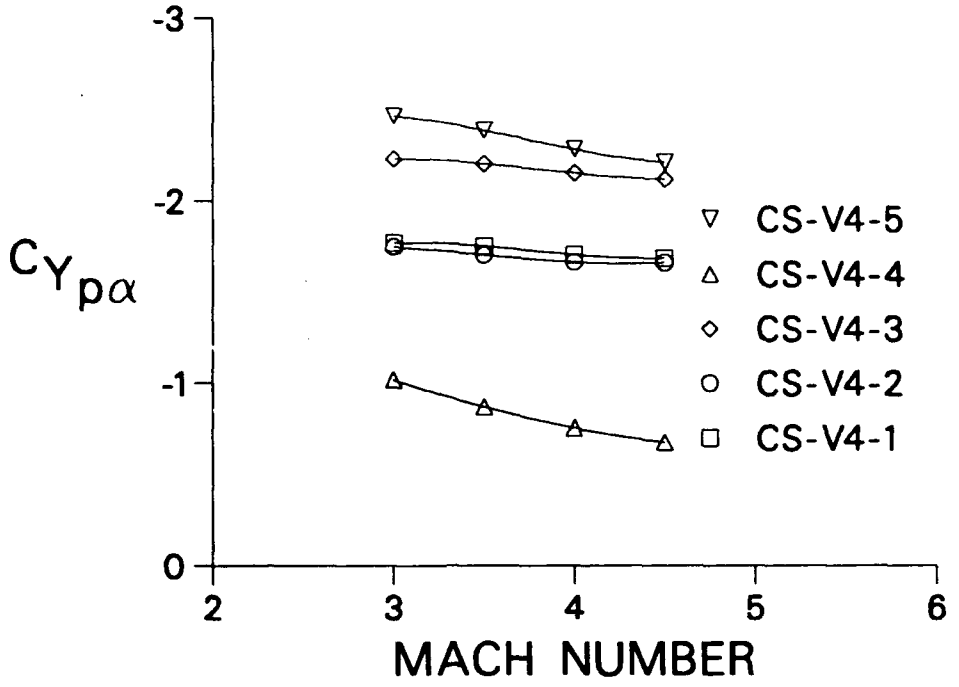

Figure 16. Variation of the Magnus force coefficient with Mach number, CS-V4-1 to CS-V4-5

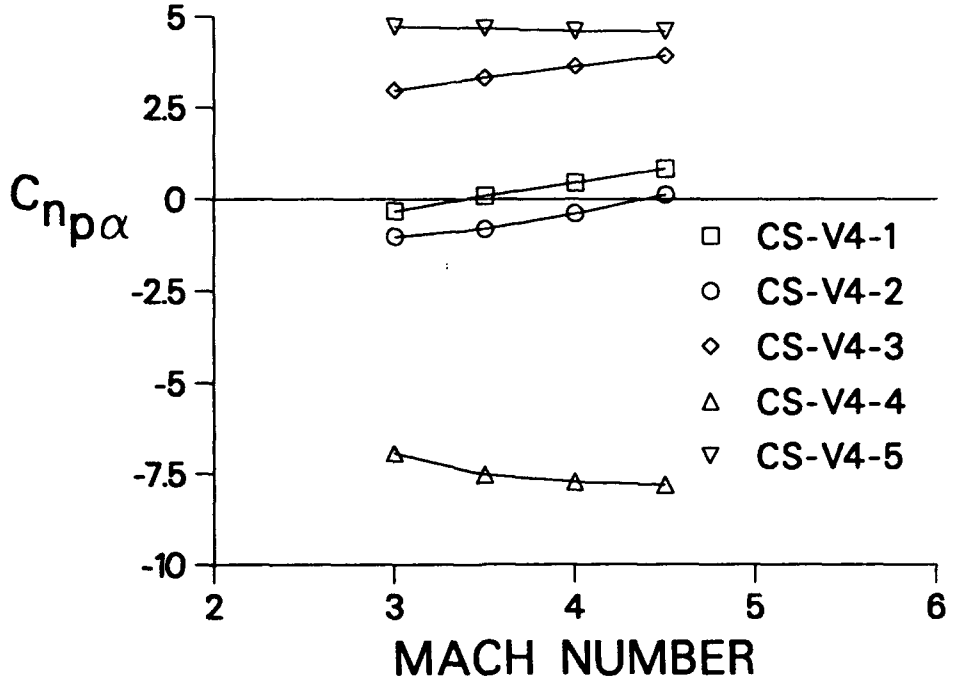

Figure 17. Variation of the Magnus moment coefficient with Mach number, CS-V4-1 to CS-V4-5

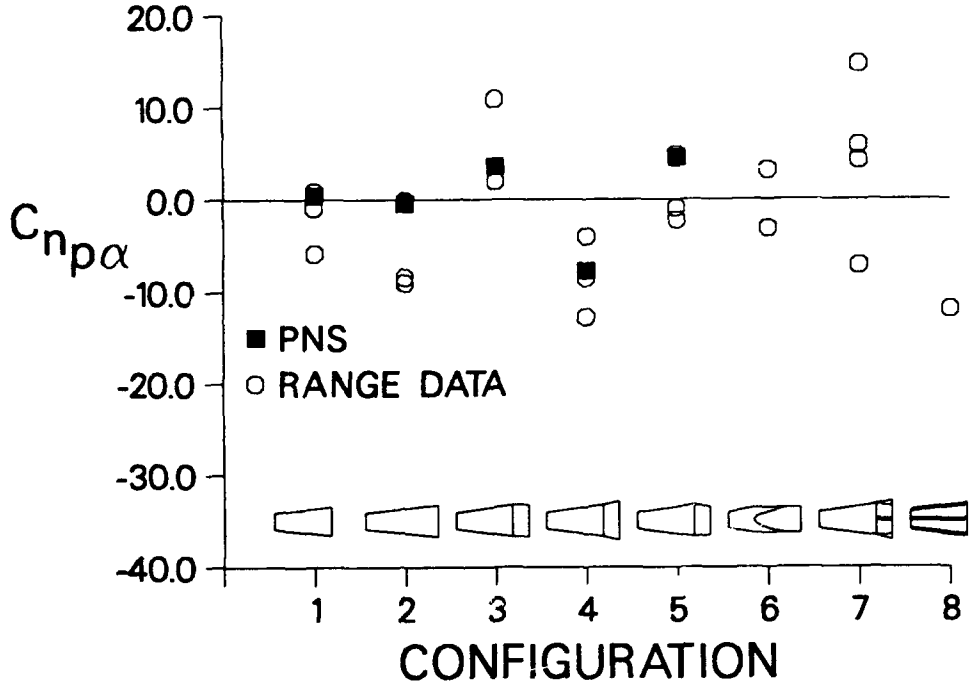

Figure 18. Magnus moment coefficient versus configuration, Mach 4

REFERENCES

1. Celmins, I., "Aerodynamic Characteristics of Fin and Flare-Stabilized 25mm XM910 Prototypes," U.S. Army Ballistic Research Laboratory, Aberdeen Proving Ground, MD, Technical Report BRL-TR-2882, December 1987. (AD 191683)

2. Danberg, J.E., Sigal, A., and Celmins, I., "Aerodynamic Characteristics of a Family of Cone-Cylinder-Flare Projectiles," Journal of Spacecraft and Rockets, Vol. 27, No. 4, July-August 1990, pp 335-360. Also see, Danberg, J.E., Sigal, A., and Celmins, I., "Prediction and Comparison with Measurements of the Aerodynamic Characteristics of Flare-Stabilized XM910 Prototypes," U.S. Army Ballistic Research Laboratory, Aberdeen Proving Ground, MD, Technical Report BRL-MR-3752, May 1989. (AD 208099)

3. Weinacht, P., and Sturek, W.B., "Navier-Stokes Predictions of Pitch Damping for Finned Projectiles Using Steady Coning Motion," AIAA Paper 90-3088, AIAA 8th Applied Aerodynamics Conference, Portland, OR, August 20-22, 1990.

4. Weinacht, P., Sturek, W.B., and Schiff, L.B., "Navier-Stokes Predictions of Pitch Damping for Axisymmetric Shell Using Steady Coning Motion," AIAA Paper 91-2855, AIAA Atmospheric Flight Mechanics Conference, New Orleans, LA, August 12-14, 1991.

5. Murphy, C.H., "Free Flight Motion of Symmetric Missiles," U.S. Army Ballistic Research Laboratory, Aberdeen Proving Ground, MD, Report No. 1216, July 1963. (AD A442757)

6. Tobak, M., Schiff, L.B., and Peterson, V.L., "Aerodynamics of Bodies of Revolution in Coning Motion," AIAA Journal, Vol. 7, No. 1, January 1969, pp. 95-99.

7. Schiff, L.B., and Tobak, M., "Results from a New Wind-Tunnel Apparatus for Studying Coning and Spinning Motions of Bodies of Revolution," AIAA Journal, Vol. 8, No. 11, November 1970, pp. 1953-1957.

8. Schiff, L.B., "Nonlinear Aerodynamics of Bodies in Coning Motion," AIAA Journal, Vol. 10, No. 11, November 1972, pp. 1517-1522.

9. Agarwal, R., and Rakich, J.V., "Computation of Supersonic Laminar Viscous Flow Past a Pointed Cone at Angle of Attack in Spinning and Coning Motion," AIAA Paper 78-1211, AIAA 11th Fluid and Plasma Dynamics Conference, Seattle, WA, July 1978.

10. Lin, T.C., "A Numerical Study of the Aerodynamics of a Reentry Vehicle in Steady Coning Motion," AIAA Paper 78-1358, AIAA Atmospheric Flight Mechanics Conference, Palo Alto, CA, August 1978.

11. Schiff, L.B., and Steger, J.L., "Numerical Simulation of Steady Supersonic Viscous Flow," AIAA Journal, Vol. 18, No. 12, December 1980, pp. 1421-1430.

12. Baldwin, B.S., and Lomax, H., "Thin Layer Approximation and Algebraic Model for Separated Turbulent Flows," AIAA Paper 78-257, 16th Aerospace Sciences Meeting, January 1978.

13. Beam, R., and Warming, R.F., "An Implicit Factored Scheme for the Compressible Navier-Stokes Equations," AIAA Journal, Vol. 16, No. 4, 1978, pp. 85-129.

14. Rai, M.M., and Chaussee, D.S., "New Implicit Boundary Procedure: Theory and Applications," AIAA Paper 83-0123, Reno, NV, January 1983.

LIST OF SYMBOLS

a_∞	free-stream speed of sound
	slope of the pitching moment coefficient with angle of attack
$C_{m_q} + C_{m_{\dot{\alpha}}}$	pitch-damping moment coefficient
C_n	side moment coefficient
$C_{n_{\dot{\phi}}}$	slope of the side moment coefficient with coning rate
$C_{n_{p\alpha}}$	Magnus moment coefficient
$C_{N_q} + C_{N_{\dot{\alpha}}}$	pitch-damping force coefficient
$C_{Y_{p\alpha}}$	Magnus force coefficient
D	projectile diameter
e	total energy per unit volume, nondimensionalized by $\rho_\infty a_\infty^2$
$\hat{E}, \hat{F}, \hat{G}$	flux vectors in transformed coordinates
$\hat{H}$	source term resulting from rotating coordinate frame
J	Jacobian
l	characteristic length, typically the projectile diameter
M_∞	free-stream Mach number
p	pressure, as used in thin-layer Navier-Stokes equations, nondimensionalized by $\rho_\infty a_\infty^2$
p	spin rate in nonrolling coordinate frame, as used in the aerodynamic moment equations and coefficients
Pr	Prandtl number
Pr_t	turbulent Prandtl number
Re	Reynolds number, $a_\infty \rho_\infty D/\mu_\infty$
$\hat{S}$	viscous flux vector in transformed coordinates
t	time
u, v, w	velocity components in x, y, and z directions, nondimensionalized by a_∞
U, V, W	Contravariant velocities of the transformed Navier-Stokes equations
V	free-stream velocity used to nondimensionalize the coning rate, spin rate, and the aerodynamic coefficients
x, y, z	axial, horizontal, and vertical coordinates with respect to the body
x_{cg}	axial location of projectile center of gravity with respect to the axial coordinate, x

Greek Symbols

α	total angle of attack
γ	ratio of specific heats, as used in Navier-Stokes equations
γ	cosine of the total angle of attack, as used in aerodynamic force and moment formulations
δ	sine of the total angle of attack
μ	laminar viscosity
μ_t	turbulent viscosity

ξ, η, ζ	transformed coordinates in Navier-Stokes equations
ρ	density, normalized by ρ_∞
ρ_∞	free-stream density
$\dot{\phi}$	coning rate of projectile
$\frac{\dot{\phi}D}{V}$	nondimensional coning rate
Ω_c	coning rate of projectile, nondimensionalized by a_∞/D

No. of Copies	Organization
2	Administrator Defense Technical Info Center ATTN: DTIC-DDA Cameron Station Alexandria, VA 22304-6145
1	Commander U.S. Army Materiel Command ATTN: AMCAM 5001 Eisenhower Ave. Alexandria, VA 22333-0001
1	Director U.S. Army Research Laboratory ATTN: AMSRL-OP-SD-TA, Records Management 2800 Powder Mill Rd. Adelphi, MD 20783-1145
3	Director U.S. Army Research Laboratory ATTN: AMSRL-OP-SD-TL, Technical Library 2800 Powder Mill Rd. Adelphi, MD 20783-1145
1	Director U.S. Army Research Laboratory ATTN: AMSRL-OP-SD-TP, Technical Publishing Branch 2800 Powder Mill Rd. Adelphi, MD 20783-1145
2	Commander U.S. Army Armament Research, Development, and Engineering Center ATTN: SMCAR-TDC Picatinny Arsenal, NJ 07806-5000
1	Director Benet Weapons Laboratory U.S. Army Armament Research, Development, and Engineering Center ATTN: SMCAR-CCB-TL Watervliet, NY 12189-4050
1	Director U.S. Army Advanced Systems Research and Analysis Office (ATCOM) ATTN: AMSAT-R-NR, M/S 219-1 Ames Research Center Moffett Field, CA 94035-1000

No. of Copies	Organization
1	Commander U.S. Army Missile Command ATTN: AMSMI-RD-CS-R (DOC) Redstone Arsenal, AL 35898-5010
1	Commander U.S. Army Tank-Automotive Command ATTN: AMSTA-JSK (Armor Eng. Br.) Warren, MI 48397-5000
1	Director U.S. Army TRADOC Analysis Command ATTN: ATRC-WSR White Sands Missile Range, NM 88002-5502
1	Commandant U.S. Army Infantry School ATTN: ATSH-WCB-O Fort Benning, GA 31905-5000
	Aberdeen Proving Ground
2	Dir, USAMSAA ATTN: AMXSY-D AMXSY-MP, H. Cohen
1	Cdr, USATECOM ATTN: AMSTE-TC
1	Dir, USAERDEC ATTN: SCBRD-RT
1	Cdr, USACBDCOM ATTN: AMSCB-CII
1	Dir, USARL ATTN: AMSRL-SL-I
5	Dir, USARL ATTN: AMSRL-OP-AP-L

No. Copies	Organization
1	HQDA (SARD-TR/Ms. K. Kominos) WASH DC 20310-0103
1	HQDA (SARD-TR/Dr. R. Chait) WASH DC 20310-0103
2	WL/FIMC Air Force Materiel Command ATTN: Joe Manter Don Kinsey 2645 Fifth St., Ste. 7 Wright-Patterson AFB, OH 45433-7913
5	Director Air Force Armament Laboratory Aeromechanics Division Aerodynamics Branch ATTN: Mr. Gregg Abate Capt. Roger S. Gates Mr. Gerald L. Winchenbach Mr. John R. Cipolla Dr. Dave Belk Eglin AFB, FL 32542-5000
2	Commander Naval Surface Warfare Center Applied Mathematics Branch ATTN: Code R44 (Mr. F. Priolo) Code R44 (Dr. A. Wardlaw) White Oak Laboratory Silver Spring, MD 20903-5000
1	Director Sandia National Laboratories ATTN: Dr. W. Oberkampf Division 1636 Albuquerque, NM 87185
1	Commander Dahlgren Division Naval Surface Warfare Center ATTN: Dr. F. Moore Dahlgren, VA 22448-5000
1	Commander U.S. Army Armament Research, Development, and Engineering Center ATTN: SMCAR-CCH-V, Ed Fennell Picatinny Arsenal, NJ 07806-5000

No. Copies	Organization
9	Commander U.S. Army Armament Research, Development, and Engineering Center ATTN: SMCAR-LCA-F, C. Ng SMCAR-LCA-F, M. Amoruso SMCAR-LCA-F, S. Kahn SMCAR-LCA-F, J. Grau SMCAR-LCA-F, H. Hudgins SMCAR-LCA-F, W. Toledo SMCAR-LCA-F, C. Livecchia SMCAR-LCA-F, B. Wong SMCAR-LCA-F, S. Chung Picatinny Arsenal, NJ 07806-5000
1	Commander U.S. Army Armament Research, Development, and Engineering Center ATTN: AMCPM-TMA (Col. Mullen) Picatinny Arsenal, NJ 07806-5000
1	Commander U.S. Army Armament Research, Development, and Engineering Center ATTN: AMCPM-TMA-120 (C. Roller) Picatinny Arsenal, NJ 07806-5000
1	Commander U.S. Army Armament Research, Development, and Engineering Center ATTN: AMCPM-TMA-105 (C. Kimker) Picatinny Arsenal, NJ 07806-5000
1	Commander U.S. Army Missile Command ATTN: AMSMI-RD-SS-AT, B. Walker Redstone Arsenal, AL 35898-5010
1	U.S. Army Research Office ATTN: T. Doligowski P.O. Box 12211 Research Triangle Park, NC 27709-2211
3	Director National Aeronautics and Space Administration Ames Research Center ATTN: M/S N227-8, L. Schiff M/S N258-1, D. Chaussee M/S N258-1, G. Molvik Moffett Field, CA 94035

DISTRIBUTION LIST

No. Copies	Organization
1	University of Maryland Department of Aerospace Engineering ATTN: Dr. J.D. Anderson, Jr. College Park, MD 20742
1	University of Texas Department of Aerospace Engineering and Engineering Mechanics ATTN: Dr. D.S. Dolling Austin, TX 78712-1055
3	Institute for Advanced Technology ATTN: Dr. W.G. Reineke Dr. T. Kiehne Dr. D. Barnette 4030-2 W. Braker Lane Austin, TX 78759-5329
1	Science Applications, Inc. Computational Fluid Dynamics Division ATTN: Dr. D. W. Hall 994 Old Eagle School Road Suite 1018 Wayne, PA 19087
1	McDonnell Douglas Missile Systems Co. ATTN: F. McCotter Mailcode 306-4249 P.O. Box 516 St. Louis, MO 63166-5016
1	Arrow Technology Associates ATTN: Robert Whyte P.O. Box 4218 Burlington, VT 05491-0042
2	VRA Inc. ATTN: Dr. C. Lewis Dr. B.A. Bhutta P.O. Box 50 Blacksburg, VA 24063
2	Alliant Techsystems ATTN: Mark W. Swenson Richard J. Buretta Mail Station MN11-2626 600 Second Street, North East Hopkins, MN 55343
3	Martin Marietta Astro Space ATTN: Dr. James E. Daywitt Dr. David Szostowski Dr. Robert Brewer Mail Stop U-4019 Mall Blvd King of Prussia, PA 19406
2	Kaman Sciences Corp. ATTN: R. Prozan T. Hayden P.O. Box 7463 Colorado Springs, CO 80933-7463

Aberdeen Proving Ground

No. Copies	Organization
14	Dir, USARL ATTN: AMSRL-WT-W, Dr. C. Murphy AMSRL-WT-WB, Dr. W. D'Amico AMSRL-CI-C, Dr. W. Sturek AMSRL-WT-P, Mr. A. Horst AMSRL-WT-PB, Dr. E. Schmidt AMSRL-WT-PB, Dr. P. Plostins AMSRL-WT-PB, Mr. V. Oskay AMSRL-WT-PB, Mr. C. Nietubicz AMSRL-WT-PB, Dr. J. Sahu AMSRL-WT-PB, Mr. P. Weinacht AMSRL-WT-PB, Mr. H. Edge AMSRL-WT-PB, Mr. B. Guidos AMSRL-WT-PB, Mr. E. Ferry AMSRL-WT-PB, Ms. K. Heavey
1	Cdr, USARDEC ATTN: SMCAR-FSF-T, Mr. B. McCoy (Bldg. 120)

INTENTIONALLY LEFT BLANK.

USER EVALUATION SHEET/CHANGE OF ADDRESS

This Laboratory undertakes a continuing effort to improve the quality of the reports it publishes. Your comments/answers to the items/questions below will aid us in our efforts.

1. ARL Report Number ARL-TR-591 Date of Report October 1994

2. Date Report Received _____

3. Does this report satisfy a need? (Comment on purpose, related project, or other area of interest for which the report will be used.) _____

4. Specifically, how is the report being used? (Information source, design data, procedure, source of ideas, etc.) _____

5. Has the information in this report led to any quantitative savings as far as man-hours or dollars saved, operating costs avoided, or efficiencies achieved, etc? If so, please elaborate. _____

6. General Comments. What do you think should be changed to improve future reports? (Indicate changes to organization, technical content, format, etc.) _____

CURRENT ADDRESS

_____
Organization

_____
Name

_____
Street or P.O. Box No.

_____
City, State, Zip Code

7. If indicating a Change of Address or Address Correction, please provide the Current or Correct address above and the Old or Incorrect address below.

OLD ADDRESS

_____
Organization

_____
Name

_____
Street or P.O. Box No.

_____
City, State, Zip Code

(Remove this sheet, fold as indicated, tape closed, and mail.)
(DO NOT STAPLE)

DEPARTMENT OF THE ARMY

OFFICIAL BUSINESS

NO POSTAGE
NECESSARY
IF MAILED
IN THE
UNITED STATES

BUSINESS REPLY MAIL
FIRST CLASS PERMIT NO 0001, APG, MD

Postage will be paid by addressee

Director
U.S. Army Research Laboratory
ATTN: AMSRL-OP-AP-L
Aberdeen Proving Ground, MD 21005-5066